A New Paradigm for Detecting Tsunamis by Remote Sensing

Lin, F. C.,[1] Na Nakornphanom K.,[2] **Sookhanaphibarn, K.,**[3] **and Lursinsap, C.,**[4]
Advanced Virtual and Intelligent Computing (AVIC) Center, Chulalongkorn University, Bangkok, Thailand
E-mail: linbfrank@gmail.com,[1] nkodchakorn@hotmail.com[2], kingkarn@ieee.org[3], lchidcha@chula.ac.th[4]

Abstract
We show that a geostationary satellite in the infrared domain can 'see' an erupting tsunami at its epicenter. The tsunami magnitude is defined and calibrated in infrared space.

1. Introduction

Present methods such as "The Deep-ocean Assessment and Reporting of Tsunami" (DART) to detect tsunamis measure aquatic pressure changes due to submarine earthquakes. The DART system functions as follows: Pressure sensors are placed at the ocean bottom near the earthquake zone. An acoustic modem transducer encodes the data into sound waves. A communications buoy processes the information and sends it by radio waves to a weather satellite (GOES). Computers at ground station calculate tsunami's starting point, speed and arrival times. The pressure changes, however, may not trigger a tsunami, and consequently the present method yields high rates of false positive alarms. According to Gonzalez (1999) and others, approximately 75% of all warnings issued since 1948 have been false. In this paper we present a direct, novel and *more economical* method, which promises, in conjunction with the earthquake detection, to give unequivocal results. We focus on the gigantic tsunami in the Indian Ocean on Dec. 26, 2004. The thermo cline of the Indian Ocean decreases from around 25 deg at the surface to circa 5 deg one kilometer below the surface, and eventually attains 4 deg ten kilometers below. At the onset of the tsunami event, the cold water is lifted up to the surface. The tsunami burst is therefore characterized by a temperature gradient. Metcorological satellites such as the Chinese FY-2C, which is geostationary at Lon 105 and Lat 0 deg and recording between the frequencies 3.5 and 12.5 μm will be able to detect this temperature gradient. For this satellite, the temperature resolution is 0.5K and space resolution is 5 km. The central question that we address in this paper is this: If an undersea earthquake has been detected, say by Pacific Marine Environmental Laboratory (PMEL) or another watchdog, how can we determine if a tsunami has been generated by this earthquake? We show that an infrared geostationary satellite can 'see' the tsunami at its epicenter. At present, we do not take into account the *propagation* of the tsunami, only its *detection* at the epicenter. The presentation of the material is organized as follows: We select seven undersea earthquakes from Dec. 26th 2004, including the Main Event at Banda Aceh. The attributes of these earthquakes are listed in Table I. We then show that there is no cloud (Figure 2) and no land mass (Figure 8) above the earthquake epieenters. Subsequently, we examine each event by displaying the Signal and Wavelet Diagram at the latitude of the event one hour before the earthquake in question, then at the time of the earthquake. To read these diagrams it is only necessary to inspect the tsunami Signal (or its absence) *at the epicenter (See Table 1 for the x-coordinate)*. The other spikes, which depict noise arising, e.g., from land mass or cloud formation not at the epicenter, are not relevant to this study.

2. Representation of Tsunamis

Since this study is the first to investigate this phenomenon, we shall use two representations for each event. We emphasize again that for both representations, the only relevant spike is the one *at the location of the undersea earthquake*, which indicates that undersea water has reached the surface of the ocean thereby capable of generating a tsunami. The tsunami, however, may not propagate very far from the epicenter, and may not have been detected. The representation chosen must exhibit the tsunami signal if present and none if not. We use the following representations in this study: The Signal Diagram and the Wavelet Diagram. The Signal Diagrams are extracted directly, without intermediate processing, from the satellite images. The Signal strength (S) at each epicenter is also given in Table 1. This is simply the value of the pixel, or pixel brightness, at the epicenter. We have included two satellite images (Figure 2 and Figure

A11) in this paper so that the reader can him/herself verify the accuracy of our procedure. No other data is used. Since the raw data is the satellite image itself, no information is lost, but the result tends to be noisy. The second representation we chose is the Wavelet Diagram, which is a function of scale and time (Percival and Walden, 2000). Wavelet analysis is capable of revealing aspects of data such as trends, breakdown points, and discontinuities in higher derivatives. In addition, because it provides a different view of data than those given by other techniques such as Fourier analysis, wavelet analysis can often compress or denoise a signal without appreciable degradation. By definition, the wavelet transform of a time series f is given by:

$$W_f(a,b) = \int f(u)\, \psi^*_{a,b}(u)\, du \quad a>0$$

Equation 1

where;

$$\psi_{a,b}(u) = \frac{1}{\sqrt{a}}\, \psi(u-b/a)$$

is a ***mother-wavelet***. Here a is the scale parameter and b the translation parameter. We offer in the following a heuristic argument to justify our choice. Equation (1) can be interpreted as the correlation between f and $\Psi_{a,b}$, and W_f the correlation coefficient if normalized. If we choose a step function, such as the Haar function to be our mother wavelet, then a maximum correlation can be obtained if $f(u)$ is also a step function. In the language of tsunami detection, the wavelet coefficient $W_f(a,b)$ will exhibit a spike if $f(u)$ is characterized by an abrupt temperature gradient. And this is indeed what we observe.

3. Noise Signal

On Dec. 26, 2004 an earthquake 120 km from Banda Aceh at Lon 95.78 and Lat 3.3, Sumatra, measuring 9.0 on the Richter scale set off a devastating tsunami in the Indian Ocean. The tsunami started at 7:58:49 am local time (0:58:49 UTC) and reached Thailand at 9:45 am. Some 200,000 Coastal residents were killed and immense property damage was inflicted. In order to demarcate the boundaries of the cloud, we constructed a histogram (Figure 1) (Cayula and Cornillon, 1992), (Cornillon and Ullman, 2000) of pixel brightness, from which we determined extemporarily that for pixel brightness<40 the region is likely a shadow, for 40<pixel brightness<60, the region is likely the ocean, for 60<pixel brightness<100 the region is probably cloud and for pixel brightness>100 the region is definitely cloud. In Figure 2 we show the Indian Ocean satellite image, where the definitely cloud region has been colored white.

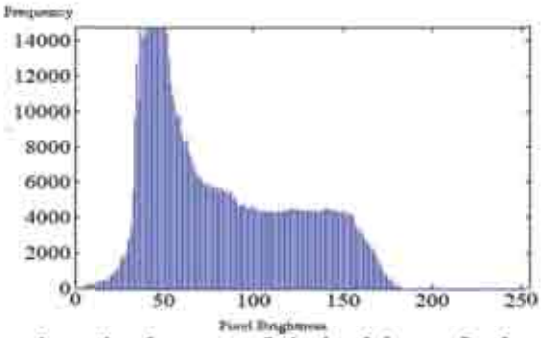

Figure 1: Histogram of Pixel Brightness for the Indian Ocean on Dec.26, 2004

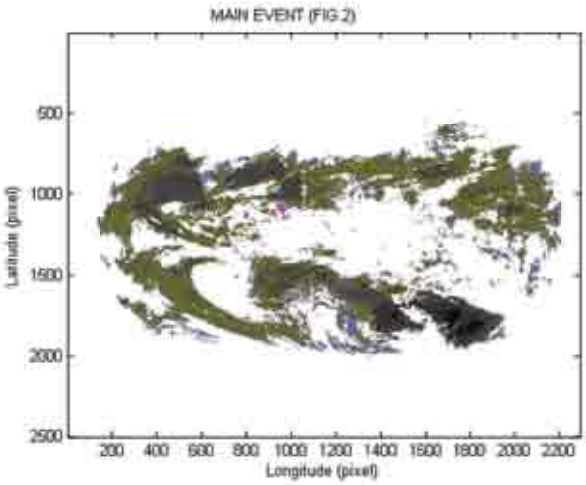

Figure 2: Satellite view of the Indian Ocean showing cloud cover at 8 am. Main Event is at LAT 3.3 (1067 pixel) & LON 95.8 (966 pixel)

The approximate location of Banda Aceh is designated by a dot, which in the picture has the image location of pixel x=966 and y=1067. We note that Figure 2 is the sole database upon which subsequent analysis for the Main Event is based, as the reader can readily verify. When we refer to Banda Aceh, we mean the epicenter of the Main Event. From Figure 2 we verify that the locations being investigated are not under cloud cover. We have also considered the possibility that for pixel brightness>80 the region is definitely cloud. In that case there is no significant deviation from Figure 2, except for a patch adjacent to Western Australia, which, however, does not concern us here. Most noise that interferes with the tsunami signal arises from temperature gradients from the clouds. Other possible sources of noise may be, for instance, heat emanating from land mass. We ascertain that the tsunami signal *at the epicenter* cannot be confused with noise from cloud and/or from land (See Figure 2 and Figure 8). In this paper we utilize the thermal infrared channel IR1, which 'sees' radiation between 10.3 and 11.3 μm, *exclusively*.

However, we also show below (Figure 3) the Main Event (the equivalent of Figure 5 in IR1) using IR channel 2, with a bandwidth between 11.5 and 12.5 μm:. It is seen that at the position indicated by a triangle (LAT 3.298 deg and LON 95.779 deg) where the Main Event took place, there is no tsunami spike in IR2, confirming that the radiation is *within a narrow band and thermal in nature*. Over open ocean the brightness temperature of IR1 is greater than 267°K. In the following, we discuss the Signal and Wavelet Diagrams for the Main Event and the Sumatra aftershock individually.

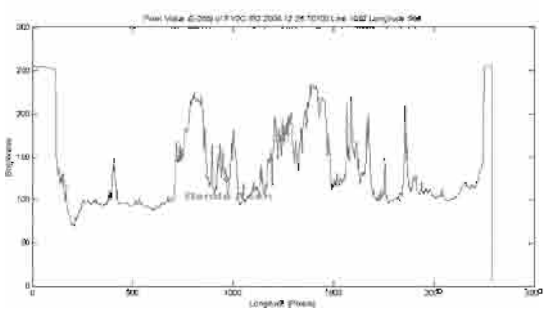

Figure 3: The (Missing) Main Event in channel IR2 (1067 pixels) at 8 a.m

4. Detection of the Main Event: (Location 1 in Figure 8):

In Figures 4 and 5 we show the signals, i.e. the infrared radiation detected by the FY-2C on Dec.26, 2004, along the latitude of Banda Aceh, at 7 am and 8 am local time respectively. Because of the temperature gradient of the thermo cline, we expect that the tsunami signal will show up in the latter figure but not the former. By comparing Figures 4 and 5, we observe that at the location of Banda Aceh, a very strong signal appears at 8 am local time (pointed to by arrow in Figure 5) which is *absent at 7 am* (Figure 4). ***Given the time and the location of the spike***, there is no doubt that this is the tsunami signal. Comparison with Figure 2 shows that towards the East we encounter the land masses Thailand and Malaysia respectively, whereas towards the West we find extensive cloud cover. In order to recognize the temperature gradient we applied a discrete wavelet analysis to latitude y=1067 pixel from the top, using the Haar mother wavelet at the 3rd detail level. The Haar mother wavelet has the constant amplitude one, and does not distort the signal. The tsunami signal is characterized by a localized spike (between 800 and 900 pixels on the x-axis) indicating a strong transient signal. The detail decompositions for Latitude 1067 pixels, at 7 am (Figure 6) and at 8 am (Figure 7) are shown below. While these representations do not convey new information, their bare bone structure facilitates direct comparison with the satellite image Figure 2. The tsunami signal is clearly discernable at the location Banda Aceh (see arrow). Regarding the horizontal scale, all Signal Diagrams encompass 500 pixels between notches and all Wavelet Diagrams span 200 pixels between notches. For the vertical scale, the range of Signal Diagrams is from 0 to 250, and the range for Wavelet Diagrams is from -100 to +100 unless otherwise labeled. In Table 1 we list the data for these aftershocks along with those of the main shock (Location 1 in Figure 8), and in Figure 8 we show the geographical locations of those epicenters under consideration. Latitudes and longitudes are given both in degrees and in pixels.

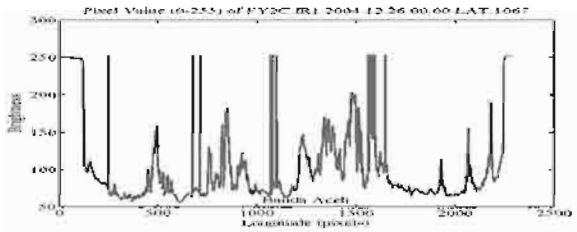

Figure 4: Signal along latitude 1067 pixels (Banda Aceh) at 7

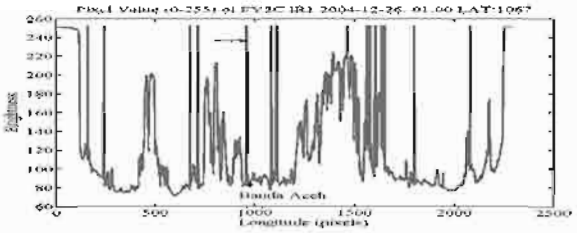

Figure 5: Signal along latitude 1067 pixels (Banda Aceh) at 8 am

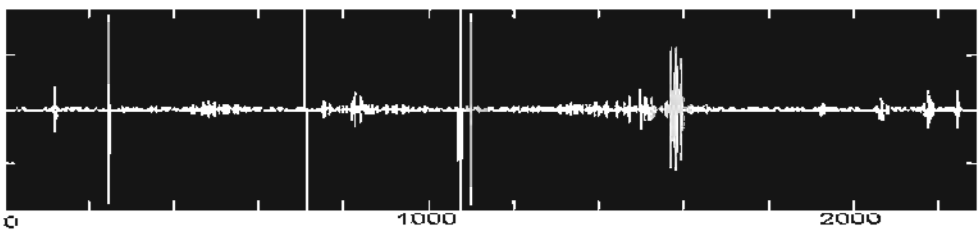

Figure 6: Wavelet Decomposition at Latitude 1067 pixels, 7 a.m

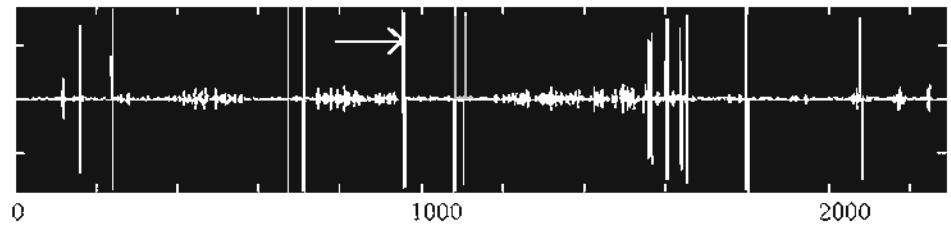

Figure 7: Wavelet Decomposition at Latitude 1067 pixels, 8 a.m

Table 1: Earthquake Epicenters

Event	M_s	Time (UTC)	Latitude	LAT in (pixels)	Longitude	LON in (pixels)	Signal at Epicenter (S in pixels)	M_t (Eq.2)
1.Mainshock	8.9	00:58:51	3.298	1067	95.779	966	417	8.7039
2.Sumatra aftershock	5.9	02:59:12	3.177	1027	94.259	950	465	8.8611
3.Nicobar	6.5	09:20:01	8.867	1043	92.382	946	461	8.8486
4.Andaman-1	5.7	07:07:10	10.336	1012	93.756	958	477	8.8978
5.Andaman-2	5.8	07:38:25	13.119	978	93.051	958	none	
6.Andaman-3	6.3	11:05:01	13.542	965	92.877	955	none	
7.Andaman-4	5.7	06:21:58	10.336	1012	92.323	945	479	8.9039

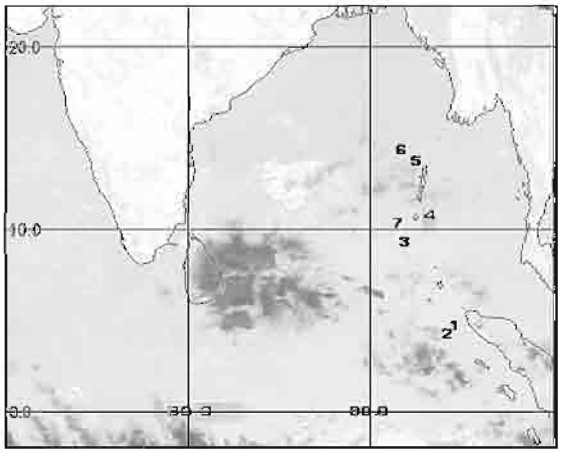

Figure 8: Location of Aftershock epicenters

5. Detection of Sumatra Aftershock: (Location 2) There are more than fifteen major aftershocks after the main shock. Most of these, however, are inaccessible either due to cloud cover, or difficulty in determining the exact location reliably. Some of these may not have triggered a tsunami (Lin and Mohamed, 1999) (Lin and Panikkar, 1995). Here we will consider an aftershock with magnitude 5.9 on 2004/12/26 at latitude 3.177 deg and longitude 94.259 deg and at 02:59 UTC near the Western coast of Northern Sumatra. (Location 2 in Figure 8). Using our methodology, it is possible to determine whether a tsunami is set in motion by this aftershock. If so, and in conjunction with a simultaneous earthquake report, we will have confidence that *a tsunami warning should be issued.* The location of the aftershock is marked by a triangle in the figures. The arrow in Figure 10 points to the tsunami signal as captured by the FY-2C, and *is absent in Figure* 9.The implication is that a *mini*-tsunami was triggered by the aftershock. This may have important consequences for water movement in the vicinity of the aftershock some two hours after the main shock, which may otherwise have been overlooked. The detail wavelet decomposition at level one is shown in Figures 11 and 12, corresponding to 9 a.m. and 10 a.m. respectively.

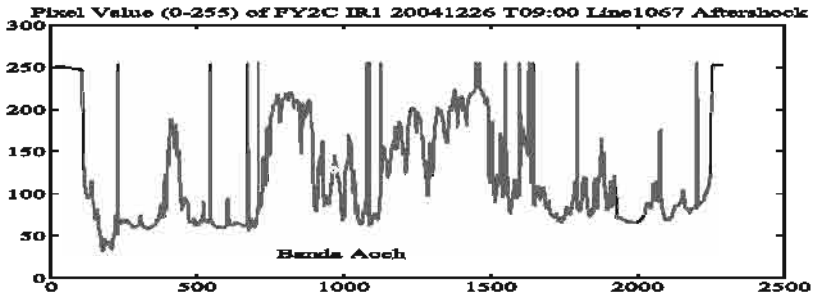

Figure 9: Signal from the Aftershock at 09:00 a.m

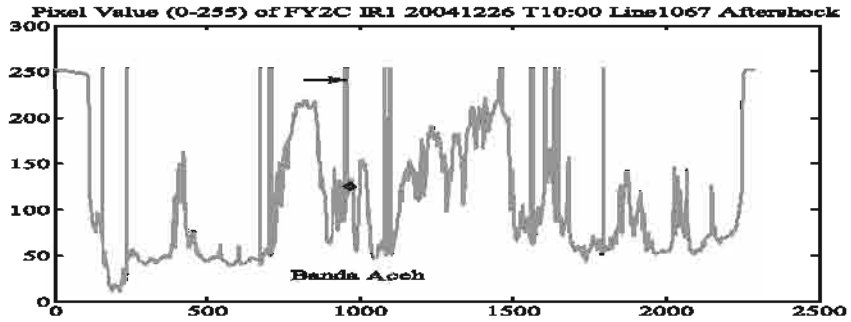

Figure 10: Signal from the Aftershock at 10:00 a.m

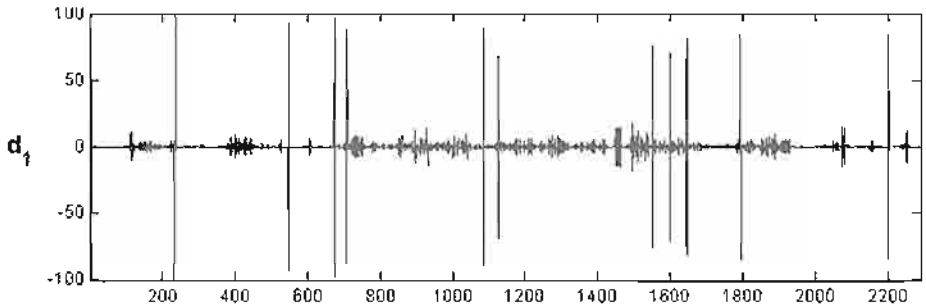

Figure 11: Detail Decomposition of Aftershock Signal at 0900 and Latitude 1067 pixels

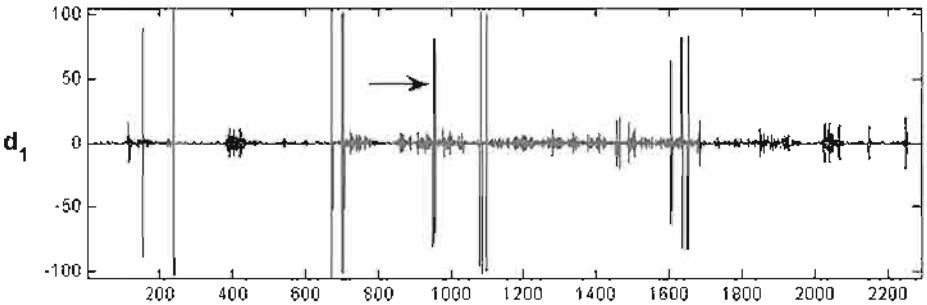

Figure 12: Detail Decomposition of Aftershock Signal at 1000 and Latitude 1067 pixels

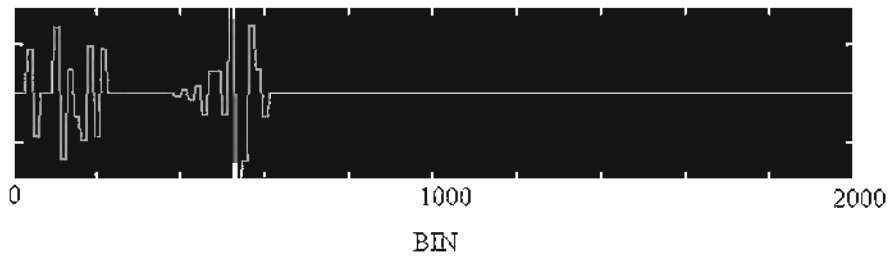

Figure 13: Detail Wavelet decomposition of NOAA night image

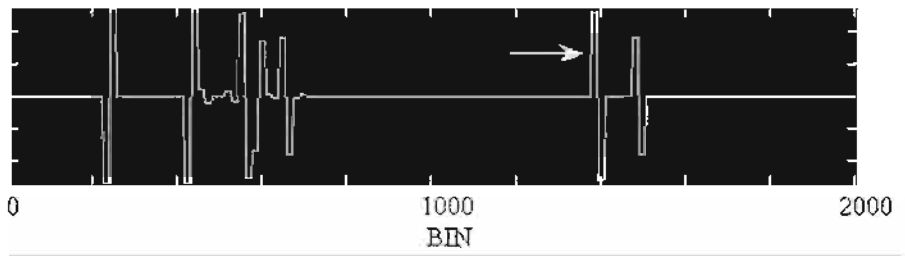

Figure 14: Detail wavelet decomposition of NOAA day image

The tsunami signal is marked by an arrow in Figure 12, but is absent in Figure 11. For comparison we reproduce previous results (Na Nakornphanom et al., 2007) obtained using deelouded IR images from the NOAA V5 Pathfinder satellite. These images are daily eomposites, whieh are defined as spatial bins of *all temperature retrievals* at a maximum resolution of 9 km. The Detail Wavelet Decomposition of the Day Image is shown in Figure 14. As indicated by the arrow, the prominent spike is interpreted to be the main shoek of the Dee.26 2004 tsunami. The accompanying minor spike is the aftershock approximately two hours after the main shock at the same latitude. *These tsunami signals are absent* in the Night Image (Figure 13). Since these images are cumulative composites, the separation between the main event and the aftershock corresponds to an approximate two-hour' rotation of the earth. A two-dimensional Time Series can be constructed using the Wavelet Diagrams Figure 6 (7 a.m.), Figure 7 (8 a.m.), Figure 11 (9 a.m.) and Figure 12 (10 a.m.) at latitude 3.2 (1067 pixels). It is seen that the tsunami signal dissipates rapidly as the eold water is mixed with the oeean surfaee water. In **Appendix A** we shall consider several aftershoeks after the main shock on the same day along the Andaman-Nieobar rupture. We apply the same analysis in order to test the validity of our procedure, to gain empirical insight into the nature of the eruption locally such as its magnitude and intensity, and possibly, to identify the direction of future research. *The interesting result is that two of the four aftershocks did not generate a tsunami.*

6. Tsunami Magnitude

We define the Tsunami Magnitude *in infrared space*, in analogy to the definition of Iida et al., (1967) in visible space, as follows:

$$M_t = log_2 S$$

Equation 2

where:
M_t = Tsunami Magnitude,
S = Tsunami Signal (Pixcl brightness at the epicenter. Sec Tablc 1 for numerical valucs obtaincd directly from the satellite images). Similarly, the Tsunami Intensity can be defined as:

$$I_t = log_2(\sqrt{2} * S)$$

Equation 3

In visible space (Rastogi and Jaiswal, 2006) S is the estimated maximum run up height of the wave. This measure has been suggested based on the effeet and damage eaused by the tsunami. The veloeity of a tsunami in the open ocean is given by

$$V = (dg)^{1/2}$$

Equation 4

where d is the ocean depth and g the acceleration of gravity. Iida (1958) also found a linear relationship between the earthquake magnitude and the tsunami magnitude in visible space, as follows:

$$M_t = 2.61M_e - 18.44$$

Equation 5

where:
M_t = Tsunami magnitude, and
M_e = Earthquake magnitude.

As in the case of Iida, the earthquake and infrared Tsunami magnitudes lie approximately on a straight line. The equation for a least square fit is given by the following:

$$M_t = 9.2299 - 0.0592*M_e$$

Equation 6

Intuitively it is useful to regard a measure rof tsunami magnitude as an increasing function of the earthquake magnitude. We define a calibrated tsunami magnitude called the tsunami Index *I*, as follows:

$$I= 1000*log_2^{-1}(S)-110$$

Equation 7

The relationship of I to M_e is given in Figure 15 below: These results can be used to estimate the tsunami magnitude. The 'outlier' in Figure 15 is the Main Event. As we have mentioned, there are many factors that contribute to the birth of a tsunami. It appears that, in the range we are considering, they are insignificant or canccl out. In order to reduce thc 'blind interval' when the satellite image is being refreshcd it is possible to retain several geostationary satellites, such as the MTSAT-1R (which takes about 30 minutes to complete a scan), in addition to the FY-2C. In the wavelet figures the positions at which the tsunami signal is found cannot be determined exactly due to the circular shift inherent in wavelet analysis. Nevertheless, we are able to derive useful information for detection and early warning of tsunamis – a vital task.

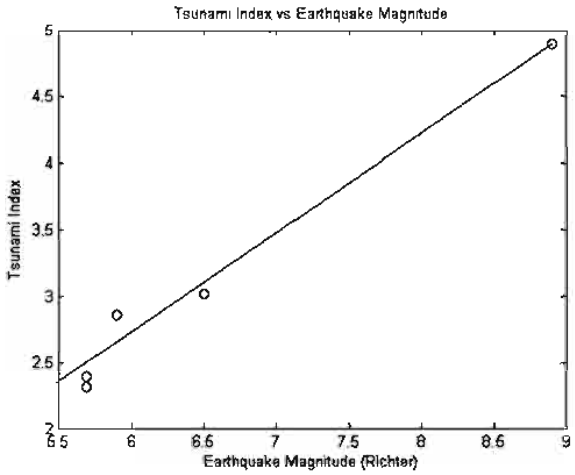

Figure 15: Earthquake *vs* Infrared Tsunami Index

7. Conclusion

We have provided *prima facie* evidence that tsunamis can be detected by geostationary satellites in the infrared domain at its epicenter. We have examined images for known earthquakes and we did indeed detect the anticipated signal. Its conclusions appear to be reliable, so that false positive alarms can be reduced in future. Since the satellite is already in place, the expenses to set up our scheme will be minimal. Also, it can be made available to most countries lacking such facility. It is expected to function with high degree of accuracy. Our procedure can be incorporated into an early warning system which potentially can save lives and property. This study may be considered as a test of concept, which seems to be sound. Since this is the first study to investigate this phenomenon, there are still outstanding questions which need to be addressed. For example, the hydrodynamic and thermodynamic mechanism by which the cool water is transported to the surface is yet unknown. Its elucidation may enable artificial constructs to be erected in its path to dissipate the tsunami. Since our premise for the Indian Ocean is a relatively warm surface temperature, our proposal may not be applicable in the polar region, such as Alaska; The question of cloud cover needs to be examined in greater detail, although in this study we are fortunate to have selected locations with a clear sky. Here we have deliberately excluded the problem of the propagation of the tsunami, which would constitute another study of equal importance. We do not know the physical extent of the cold water patch on the surface, other than that it disperses rapidly. To resolve surface dynamics it will be worthwhile to improve the resolution of the satellite. As this is a feasibility study, implementation issues have not been addressed.

Appendix A: Nicobar-Andaman Aftershocks

A1.The Nicobar Island: (Location 3)

The great Sumatra earthquake triggered aftershocks along the Andaman-Nicobar fault. The 26 December rupture appears to have involved slip of the entire plate boundary between 3°N and 15°N. The average slip in the Nicobars is 15-19 m. The previous rupture zones of 1847, 1881 and 1941 have re-ruptured. The islands have tilted down to the east and tilted up to the west during the earthquake. The southernmost Nicobars have apparently subsided 4.25 m. The two figures (Figures A1 and A2) illustrate that a *mini*-tsunami (The narrow width of the tsunami signal indicates its limited spatial extent. This is reflected in the wavelet diagram by a shorter spike) was indeed generated at 09:20:01 UTC at location LAT 1043 and LON 946 (pixels. See Table 1). Below (Figures A3 and A4) we show the Wavelet Decomposition of the signals. The tsunami signal is again clearly visible, pointed to by an arrow in Figure A4.

A2.The Andaman Islands:

The Sumatra Main Shock propagated 1300 km from its epicenter near Banda Aceh northward for about 10 minutes, corresponding to an average velocity of 2.1 km/s (Park et al., 2005). Aftershocks on Dec. 26 occur as strike-slip motion on the submarine Andaman fault to the east. The average slip in the Andamans is 7-8 m. Uplift of the western shores and subsidence of the eastern shoreline indicate that the main rupture was 140-160 km wide. In the following we shall consider four earthquake epicenters in the Andaman region. *The interesting result is that two of the four did not generate a tsunami.*

CASE 1:ANDAMAN-1 and ANDAMAN-4

LAT 1012: (Location 4 and 7):

We consider these two cases together since they are situated on the same latitude (1012 pixel). The ANDAMAN-1 occurred at 07:07:10 and the ANDAMAN-4 occurred at 06:21:58 UTC. The following figures indicate that there is no tsunami signal at 0600. At 0700, however, a tsunami signal appears at the Andaman-4 epicenter. Then, at 0800, another tsunami signal is detected at the Andaman-1 epicenter.

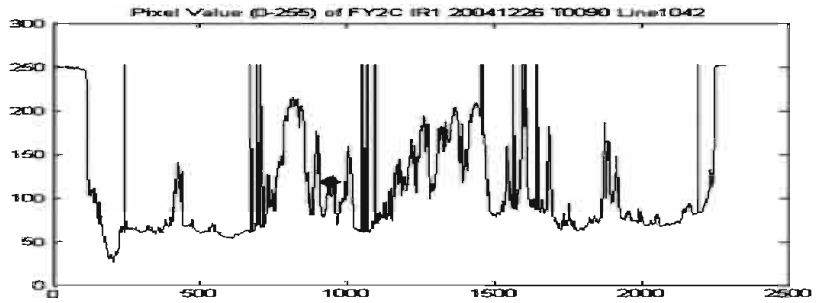

Figure A1: Signal from the Nicobar Aftershock at 0900 LAT 1042 pixels

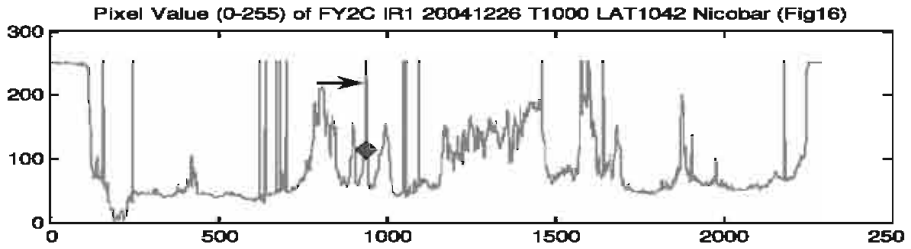

Figure A2: Signal from the Nicobar Aftershock at 1000 LAT 1042 pixels

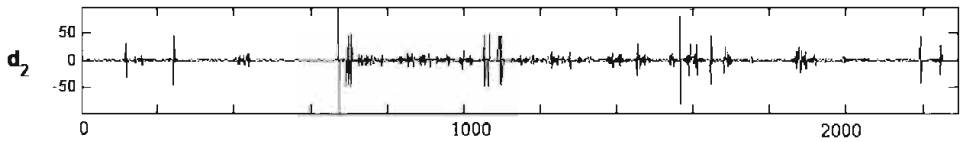

Figure A3: Wavelet Decomposition at Nicobar at 0900 LAT 1042 pixels

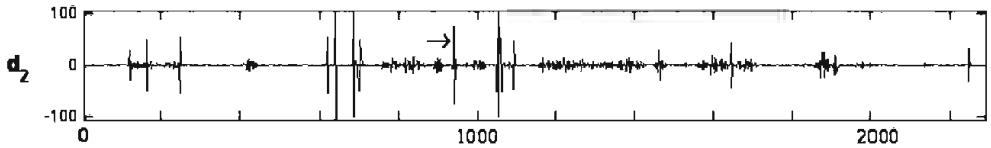

Figure A4: Wavelet Decomposition at Nicobar at 1000 LAT 1042 pixels

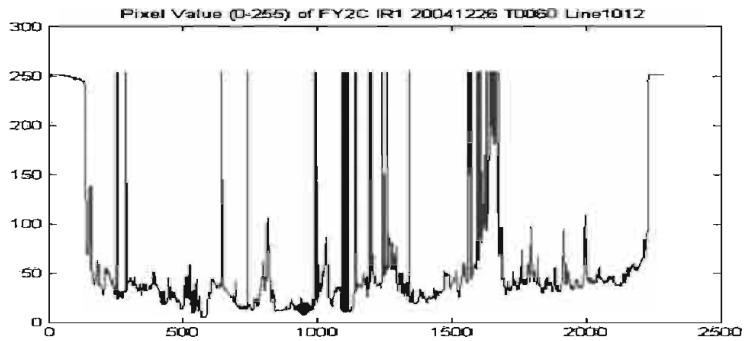

Figure A5: ANDAMAN-1 Signal 0600 LAT 1012 pixels

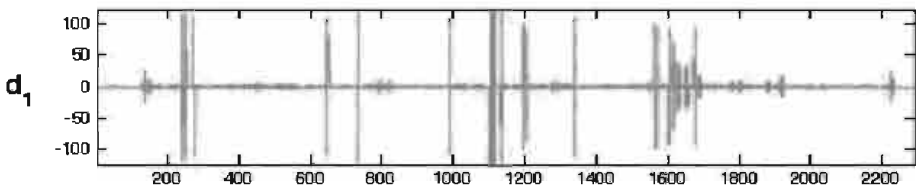

Figure A6: Wavelet Decomposition of ANDAMAN-1 at 0600 LAT 1012 pixels

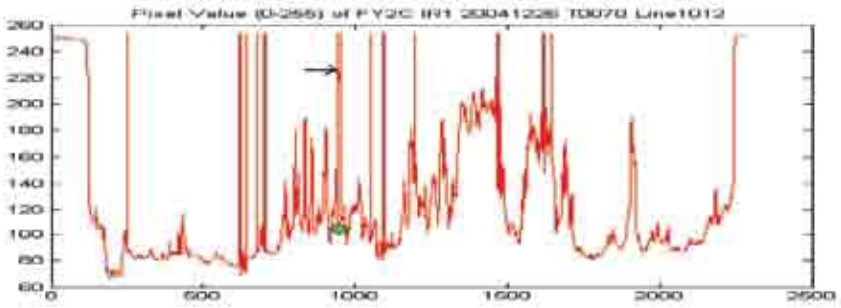

Figure A7: Signal for ANDAMAN-1 0700 LAT 1012 pixels

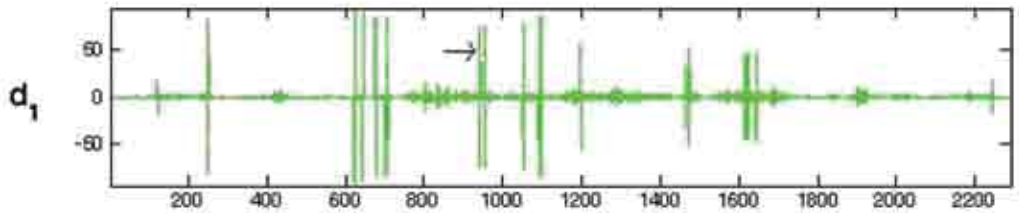

Figure A8: Wavelet Decomposition for ANDAMAN-1 0700 LAT 1012 pixels

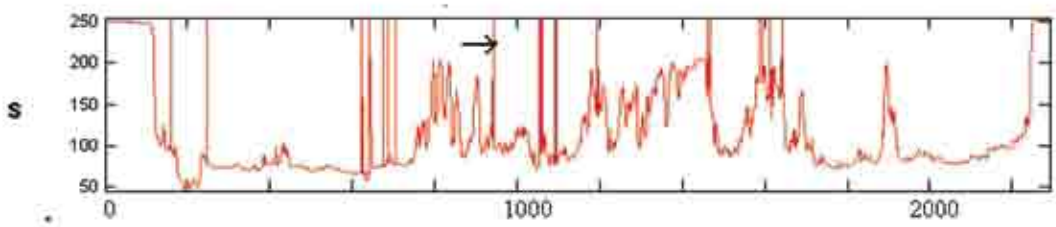

Figure A9: Signal for ANDAMAN-1 0800 LAT 1012 pixels

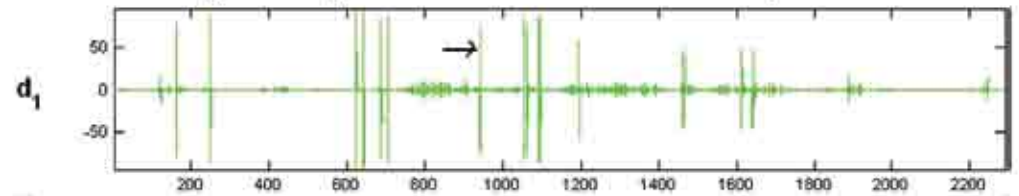

Figure A10: Wavelet Decomposition for ANDAMAN-1 0800 LAT 978 pixels

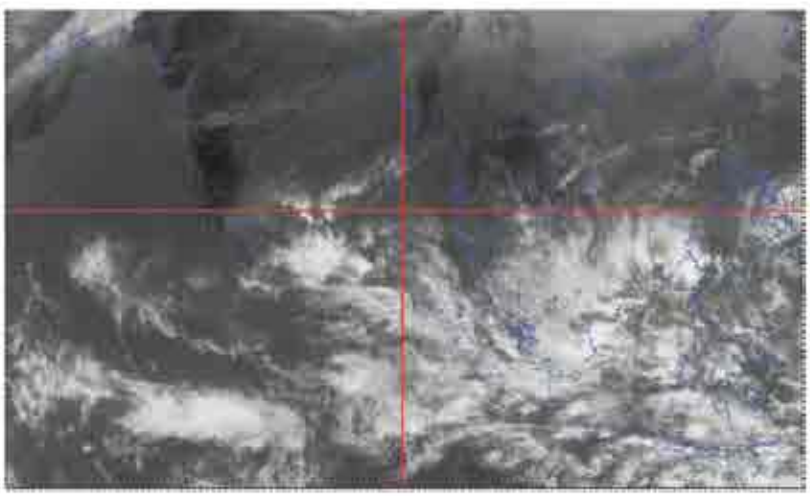

Figure A11: Satellite Photo of Epicenter for ANDAMAN-2 0800 LON 958 pixels

CASE 2: ANDAMAN-2, LAT 978: (Location 5):
The Andaman-2 earthquake occurred at 07:38:25 UTC at LAT 978 and LON 958 (See Table I). The satellite image at 0800 UTC is shown below. The following figures (A12, A13, A14, A15) show the signal and wavelet diagrams for 0700 and 0800 UTC respectively. It is seen that no tsunami is detected at this location. This is an interesting case in that there is an earthquake of magnitude 5.8 on the Richter scale which however did not spawn a tsunami. Tsunami generation depends on many other factors such as: The topology of the ocean floor, the direction of trust of a subduction zone, strong turbidity currents and the ocean depth. With our method, such false positive events can be recognized and eliminated. The database used for the above analysis is given in Figure A11, as the reader can readily verify. *No tsunami warning should be issued.*

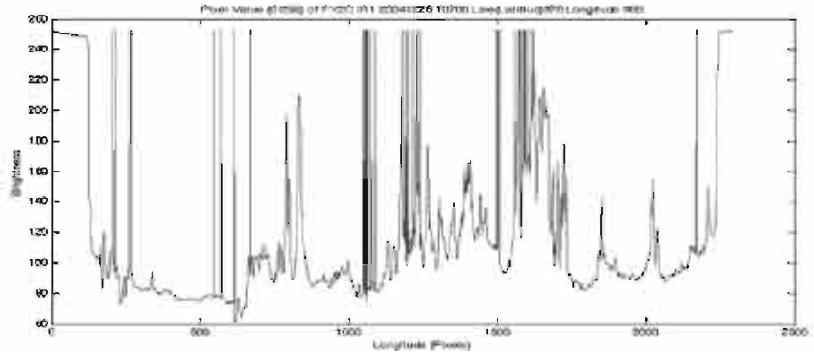

Figure A12: Signal for ANDAMAN-2 0700 LAT 978 pixels

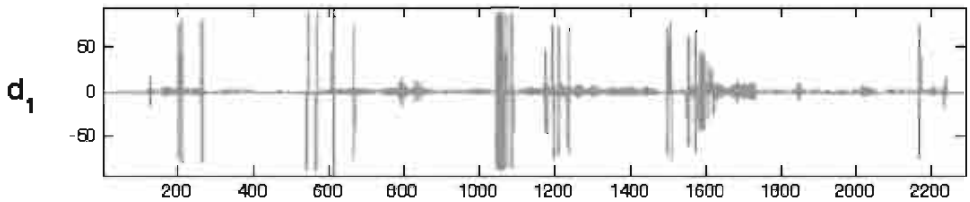

Figure A13: Wavelet Decomposition of ANDAMAN-2 0700 LAT 978 pixels

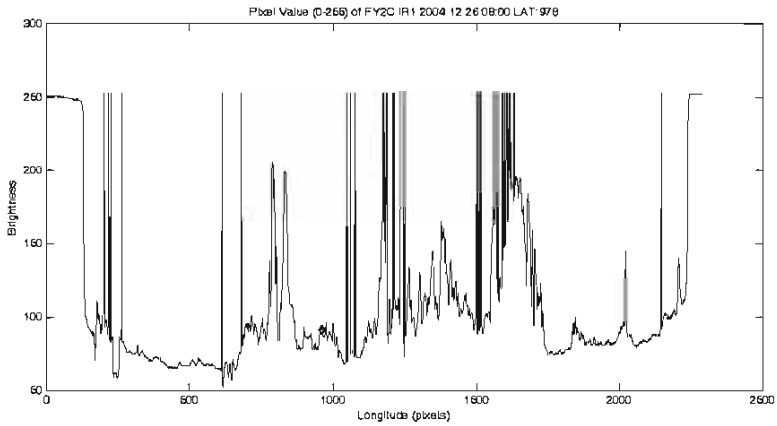

Figure A14: Signal of ANDAMAN-2 0800 LAT 978 LON 958 pixels

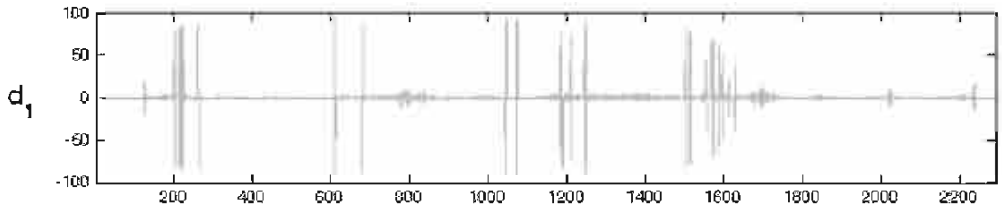

Figure A15: Wavelet Decomposition for ANDAMAN-2 0800 LAT 978 pixels

CASE 3: ANDAMAN-3, LAT 965(Location 6):
For this case, the earthquake occurred at 11:05:01 UTC at LAT 965 and LON 955. The figures below show the Signal and Wavelet diagrams at 10:56 and 11:29 UTC respectively. Again, there is no indication of a tsunami signal at this location. This is another interesting case in that an earthquake of magnitude 6.3 on the Richter scale again did not spawn a tsunami.

As mentioned earlier, tsunami generation depends on many other factors. With our method, such false positive events can be eliminated. It may be of interest to consider these factors *in situ* in order to better understand the mechanism involved which would abort a tsunami before it bursts into the ocean surface. Our methodology enables us to identify these events. In this case *no tsunami warning should be issued.*

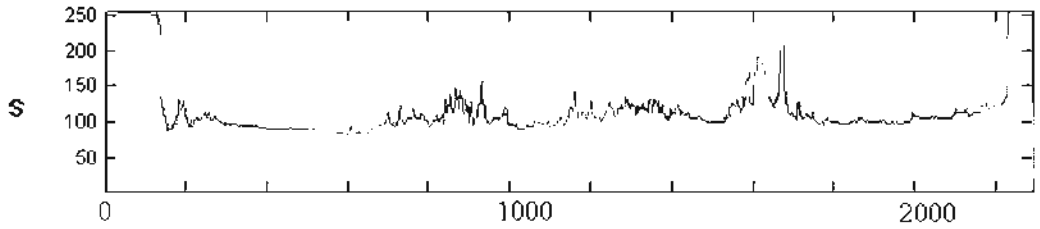

Fig.A16: Signal for ANDAMAN-3 10:56 LAT 965 pixels

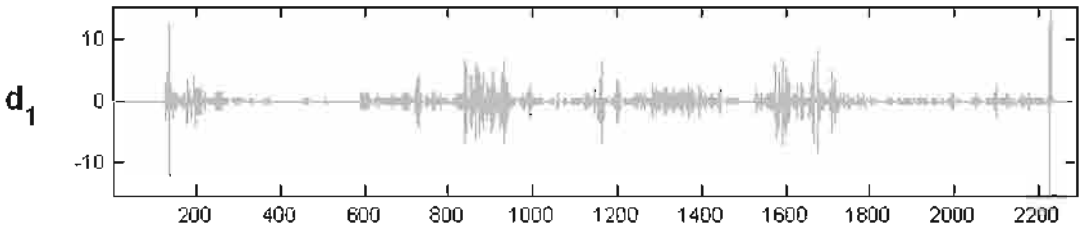

Figure A17: Wavelet Decomposition for ANDAMAN-3 10:56 LAT 965 pixels

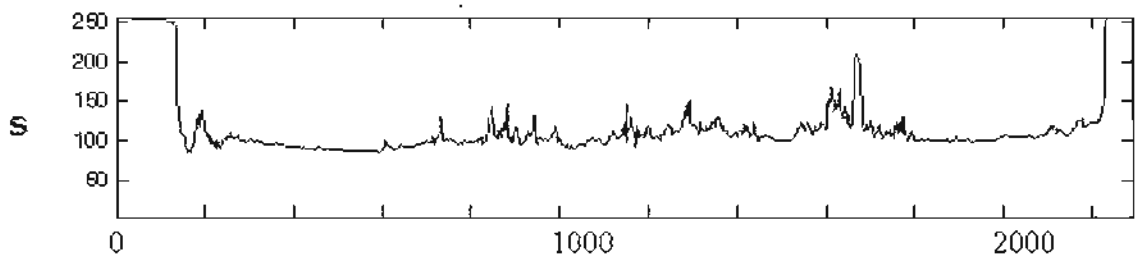

Figure A18: Signal for ANDAMAN-3 11:29 LAT 965 LON 955 pixels

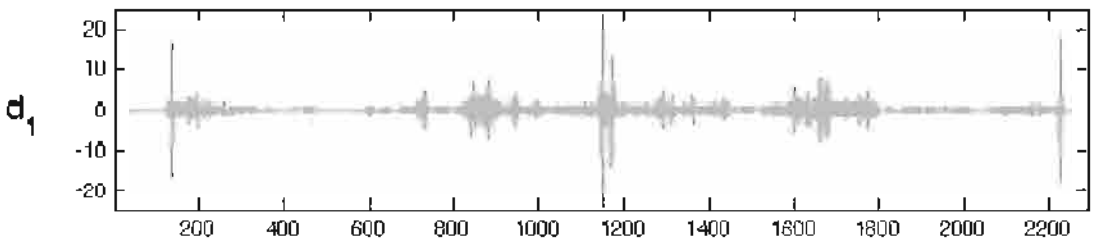

Figure A19: Wavelet Decomposition for ANDAMAN-3 11:29 LAT 965 LON 955 pixels

Acknowledgement

This work is supported in part by the Thai Research Council, Thailand. Prof. Virulh Sayakanit provided invaluable administrative support.

References

Cayula, J. F., and Cornillon, P., 1992, Edge Detection Algorithm for SST Images, *Journal of Atmospheric and Oceanic Technology*, 9 67.

Cornillon, P. C., and Ullman, D. S., 2000, Evaluation of Front Detection Methods for Satellite Derived SST Data using in Situ Observations. *Journal of Atmospheric and Oceanic Technology*, 17, No. 12, 1667.

Gonzalez, F., 1999, TSUNAMI!, Scientific American, 280, 56-65.

Iida, K.,1958 , Magnitude and Energy of Earthquakes accompanied by Tsunami and Tsunami Energy, *Journal of Earth Science*, Nagoya University, 6, No.2, 101-112.

Iida, K., Cox, D. C., and Pararas-Carayannis, G., 1967, *Preliminary Catalog of Tsunamis Occurring in the Pacific Ocean*. Hawaii Institute of Geophysics, Honolulu, HI, August (Rept. HIG- 67-10)

Lin, F. C., and Mohamed, I. E., 1999, Predicting Seismic Aftershocks using a Neural Network, in *Proceedings of the International Geoscience & Remote Sensing Symposium (IGARSS '99)*, Hamburg, Germany, 1366.

Lin, F. C., and Panikkar, I., 1995, Study of Seismic Activity in Central Asia Applying A Parallel Distributed Paradigm, in *Proceedings of the International Geoscience & Remote Sensing Symposium (IGARSS '95)*, Firenze, Italy, 2195

Na Nakornphanom, K, Lin, F. C., and Lursinsap, C., 2007, Tsunami Detection and Early Warning by TIR Remote Sensing; Abstract, *Third Shanghai International Symposium on Nonlinear Sciences and Applications*, June 6-10.

Park, J. K., Anderson, R., Aster, R., Butler, R., Lay, T., and Simpson, D., 2005, *Global Seismographic Network records the Great Sumatra – Andaman Earthquake*, Eos, 86(6), 57.

Percival, D. B., and Walden, A. T., 2000, *Wavelet Methods for Time Series Analysis*, Cambridge University Press.

Rastogi, B. K., and Jaiswal, R. K., 2006, A Catalog of Tsunamis in the Indian Ocean, *Science of Tsunami Hazards*, Vol. 25, No.3, 128.